Optimal number of rotor parameters for the automatic design of Synchronous Reluctance machines

Optimal Number of Rotor Parameters for the Automatic Design of Synchronous Reluctance Machines

Matteo Gamba, Gianmario Pellegrino, *Senior Member, IEEE*, and Francesco Cupertino, *Senior Member, IEEE*

***Abstract* -- The automatic design of Synchronous Reluctance machines is proposed, based on Multi-Objective Optimization and Finite-Element Analysis. An original description of the rotor geometry in the simple terms of three parameters per flux barrier is formalized and tested with finite elements and experiments. The results obtained with the proposed geometry are compared to the ones previously obtained applying the same automatic design procedure to simpler geometries. Plus, a state of the art rotor, designed with no restrictions in terms of geometric degrees of freedom is also used as a further benchmark for the comparison. The paper demonstrates that three variables per barrier is the appropriate number of parameters to be used for a fast and yet accurate description of multi-barrier Synchronous Reluctance machine rotors.**

***Index Terms*—AC Motors, Variable Speed Drives, Synchronous Reluctance Machines, Optimization Algorithms, Finite Element Analysis.**

I. Introduction

Synchronous Reluctance (SyR) machines are a viable alternative to variable speed Induction Motors (IM), because of their higher efficiency and transient overload capability [1]. Recently, the volatile price of rare-earth permanent magnet (PM) materials has renewed the interest towards magnet-free AC machines, such as the SyR one [2], and towards the use of low cost magnets, as is the case of ferrite-assisted SyR machines [3].

SyR machines have been studied comprehensively since the 1990s [1,4-5]. Their stators are at all extents the same of those of induction motors. Dealing with their rotors, a standard design procedure is yet an open challenge, in particular for the industry, where SyR machines are still very little known.

The automatic design of such machines by means of optimization algorithms [6-8] is discouraged by the mandatory use of finite element analysis (FEA) and to the peculiarity that more than one FEA simulation is needed for the evaluation of each new SyR machine. Both factors easily lead to long computational times. The use of FEA is mandatory because of the influence of magnetic saturation on machine performances [9]. Plus, torque ripple minimization is necessary [1,2,4,5], and this requires FEA simulations in multiple rotor positions per each machine evaluation. Last, the current phase angle giving the Maximum Torque per Ampere (MTPA) is not known a priori for every new candidate machine. All considered, the number of FEA simulations required by multi-objective optimization turns out to be quite high.

Previous work was dedicated to the simplification of the optimization problem [10] and to the quick FEA evaluation of candidate machines [11]. The former point is intended as the proper selection of the optimization goals (torque per Joule loss and torque ripple) and of the geometric variables to be optimized. The quick FEA evaluation first proposed in [11] uses five rotor positions with a random rotor offset and of a single current value with the phase angle decided by the optimization algorithm.

This paper focuses on the choice of the rotor geometric parameters. The number of geometric parameters required to describe a multi barrier SyR rotor varies in the literature, it is generally high and grows quickly with the number of layers [7,8,13]. Those who applied FEA and optimization algorithms jointly mostly experimented them on simpler geometries with one rotor barrier [8,14], or with admittedly long computational times [7,13]. Different types of simplified rotor geometries, described by two parameters for each flux barrier were tested in [12]. In this paper one additional degree of freedom is introduced per each flux barrier, so to improve the output torque per Ampere ratio at the expense of a limited extra time of computation.

The paper describes the geometric model and the optimization procedure, based on multi-objective differential evolution (MODE). The final design produced by the MODE is compared to another MODE-designed machine with a simpler rotor geometry and also to a state-of-the-art design. The comparison is presented both in simulations and experiments, using three prototypes purposely manufactured to this scope. The "fluid barrier" geometry proposed in the paper overcomes the limitations in terms of maximum torque of the former automatic designs, and gets to give more torque also of the state-of-the-art machine.

II. Proposed Fluid Barriers Geometry

The SyR rotor geometry heavily affects the torque, torque ripple and losses [1,2,4-6]. The key rotor parameters are 1) the number of flux barriers n_{lay}, 2) the position of their ends at the airgap, 3) the thicknesses of the flux barriers and the flux guides.

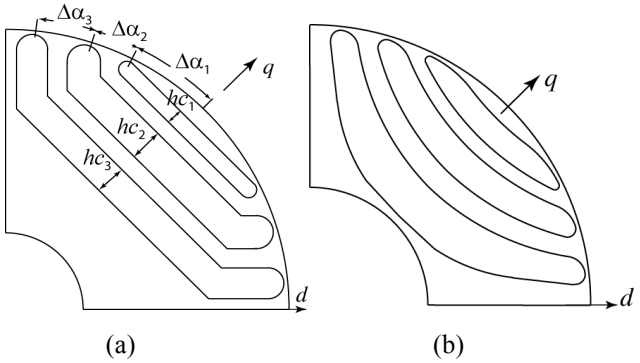

Figure 1. a) Example of rotor pole with I2U barriers [12]. b) Proposed "fluid barrier" type rotor pole.

M. Gamba and Gianmario Pellegrino are with the Politecnico di Torino, Department of Energy, Turin, Italy (e-mail: matteo.gamba@polito.it, gianmario.pellegrino@polito.it).

F. Cupertino is with the Politecnico di Bari, Electrical and Electronic Engineering Department, Bari, Italy (e-mail: cupertino@poliba.it).

In previous works the rotor barriers were described via 1) their radial thickness and 2) the angular position of their ends at the airgap, as represented in Fig. 1a. Barriers of circular and angled shapes were tested, with similar results [12]. The example of Fig. 1a refers to the angled barriers rotor called I2U (one I-shaped plus two U-shaped barriers). In this paper the barrier profiles are of the kind of the one in Fig. 1b, with one more degree of freedom per barrier accounting for the thickness of the flux guides separately from the thickness of the flux barriers.

A. *Fluid Barrier Profiles*

The automatic construction of the flux barriers was embedded into the optimization procedure by means of the Matlab scripting functionality of FEMM [15]. The profiles of the new barriers proposed here are inspired to the field lines in a virtual solid rotor, represented in Fig. 2. A closed-form expression of such field lines can be derived from the conformal mapping theory and the Joukowski air-flow potential formulation [16]. This was originally developed to describe the fluid flow paths channeled by two infinite plates forming an angle π/p and with a plug of radius a centered into the origin of the reference frame. In the solid rotor context, the plug represents the nonmagnetic shaft. The equation expressing the magnetic field potential lines of Fig 2 is:

$$C = sin(p\theta) \cdot \frac{\left(\frac{r}{a}\right)^{2p} - 1}{\left(\frac{r}{a}\right)^{p}} \quad (1)$$

where r and θ (radius and polar angle) are the polar coordinates of each point of the plane, p is the number of pole pairs of the machine, a is the shaft radius and C defines which field line is considered: the lower is C, the closer the field line is to the shaft. So each field can be selected with continuity by the proper selection of C.

For instance, to pick up the field line that intercepts the airgap at the angular coordinate α_k defined in Fig. 2, the value C_k is determined by substitution of the coordinates of point E_k (r_k, θ_k) in (1), where E stands for the end-point of the barrier. Once C_k is known, the explicit equation of the field line, in polar coordinates, is:

$$r(\theta, C) = a \cdot \sqrt[p]{\frac{C + \sqrt{C^2 + 4sin^2(p\vartheta)}}{2sin(p\vartheta)}} \qquad 0 \le \vartheta \le \frac{\pi}{p} \quad (2)$$

B. *Automated Construction of One Barrier*

The MODE algorithm selects three parameters that define the k-th barrier (k = 1 to n_{lay}): the end angular position α_k, the height of the barrier cavity hc_k and the new parameter Δx_k, that is the offset of the cavity with respect to the α_k-defined center line.

The automated construction of the flux barriers follows the flowchart reported here below. The related geometric quantities are defined in Fig. 3.

- The α_k–driven line is traced with the procedure described in the previous subsection. The value of C_k is obtained by substitution of $\theta = \alpha_k + \frac{\pi}{2p}$ and $r = \frac{d}{2}$ in (1), being d the rotor outer diameter;
- Then, the radial coordinate r_M of the mid-point M defined in Fig. 3 is determined by substitution of C_k and $\theta = \frac{\pi}{2p}$ into (2).
- From the position of M, the radial positions of the inner and the outer bound points B_1 and B_2 are derived by means of (4) and (5):

$$r_{B1,k} = r_{Mk} - \frac{hc_k}{2} \cdot (1 - \Delta x_k) \qquad \vartheta = \frac{\pi}{2p} \quad (4)$$

$$r_{B2,k} = r_{Mk} + \frac{hc_k}{2} \cdot (1 + \Delta x_k) \qquad \vartheta = \frac{\pi}{2p} \quad (5)$$

The positions of B_1 and B_2 depend on the two parameters hc_k and Δx_k, where the per-unit offset factor Δx_k varies in the range [-1, 1].

- The inner and outer profiles of the k-th barrier are the field lines defined by the two points B_1 and B_2. Substituting the coordinates of B_1 and B_2 into (1) as already done with M leads to the knowledge of C_{B1} and C_{B2}.
- Last, the two field lines corresponding to C_{B1} and C_{B2} are drawn from equation (2).

From the analysis of (4) and (5) it comes out that the barrier is hc_k thick along the q-axis, and offset radial-wise outwards or inwards by $\Delta x_k \cdot hc_k$, with respect to the virtual midline defined by the barrier-end position α_k. For example, with Δx_k = 1 the barrier is all outwards ($B_1 = M$); vice-versa with Δx_k = -1 ($B_2 = M$). If Δx_k = 0 the barrier is 50-50 split around the nominal midline.

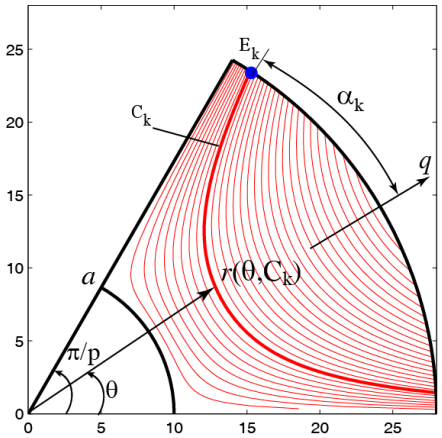

Figure 2. Field lines in a solid rotor according to conformal mapping.

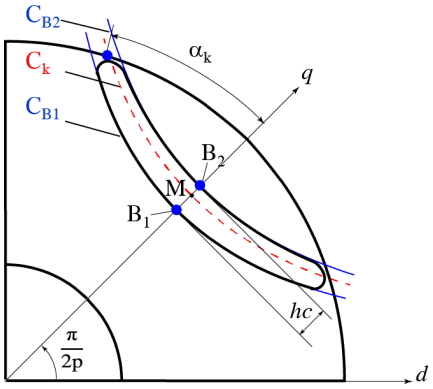

Figure 3. Construction of one rotor flux barrier.

The tangential ribs connecting the flux guides at the air-gap are traced using two circular segments tangent to the barrier side lines and to the rotor external circumference. Their thickness is minimized off-line, according to mechanical constraints (centrifugal stress) and steel cut tolerances.

C. *Automated Construction with Multiple Barriers*

When multi-barrier rotors are considered, the input data of the different barriers must be coordinated to avoid that

some combinations of the inputs lead to overlapping barriers and unfeasible rotors. At this purpose, the angles and thicknesses are expressed in normalized quantities, so that their respective sums do not exceed the available angular span ($\pi/2p$) and the available space along the q-axis, respectively. The base values of the p.u. angles and heights are the total angle of height available for all the layers. The only exception is the first angle $\Delta\alpha_1$ that is expressed in degrees and determines the angular space left to the other angular inputs: the other p.u. angles $\Delta\alpha_j$ (j = 2 to n_{lay}) define the barrier ends distribution over the remaining part of the half pole angular pitch. The p.u. thicknesses hc_{123} are interpreted as follows: if they are all 1 p.u. then the air barriers are all thick the same and occupy as much radial space as they can. The upper limit to the barriers space occupation is a minimum steel thickness of 1 mm radial-wise that is guaranteed between two adjacent barriers, to ensure that the rotors are feasible manufacturing wise. A width of 0.4 mm is used for the tangential structural ribs, connecting the flux-guides at the barriers ends. All the designed machines have been verified towards centrifugal stress via structural FEA, at the maximum speed of 8000 rpm, after the optimization. The barrier offsets Δx_{123} introduced in subsection II.B can vary between -1 and 1. The limits of the search space are summarized in Table I.

TABLE I
LIMITS OF THE SEARCH SPACE FOR THE GLOBAL SEARCH (GS) OPTIMIZATION STAGE

Parameter	Min value	Max value	Units
hc_k, k = 1 to n_{lay}	0.2	1	p.u.
Δx_k, k = 1 to n_{lay}	-1	1	p.u.
$\Delta\alpha_1$	15	27	degrees
$\Delta\alpha_j$, j = 2 to n_{lay}	0.33	0.67	p.u.
γ	20	80	degrees

TABLE II
MAIN PARAMETERS OF PROTOTYPES

Quantity	Value
Stator slots	24
Pole pairs	2
Rotor diameter	58.58 mm
Stator diameter	101 mm
Stack length	65 mm
Airgap	0.5 mm
Rated current (pk)	14.29 A
Rated voltage (dc-link)	300 V
Maximum speed	5000 rpm

III. TORQUE AND TORQUE RIPPLE OPTIMIZATION

A. Fast FEA Evaluation of the Machines

The main parameters and target ratings of the machine example are reported in Table II. Multi-objective differential evolution (MODE) and FEA are used in the following to design SyR rotors giving maximum torque and minimum torque ripple. The MODE algorithm was chosen after the comparative analysis of [8], where it showed to lead to the same rotor designs of other multi-objective optimization algorithms, but with a number of FEA calls which is consistently lower.

A single current vector in dq synchronous coordinates is simulated for each candidate machine, with the output torque evaluated in five rotor position over one stator slot pitch. The current amplitude level used in the optimization is more than twice the continuous operation current. The experience of many optimization runs over the years [12] evidenced that use of a single overload condition is much convenient than the use of a single light load condition for obtaining a torque ripple optimization that is consistent also out of the current loading level used during the optimization. To the authors' opinion this is related to the fact that the torque ripple grows very fast with the grade of saturation of the machine, so it is more significant to refer to heavy saturated conditions rather than the opposite.

The current phase angle γ (phase angle of the current vector respect to the d axis) should possibly be the one giving the maximum torque per Ampere (MTPA) condition, γ_{MTPA}, because this would maximizes also the torque per Joule loss and then, in a way, the efficiency. The phase angle γ is directly optimized by the MODE at once with the torque maximization.

B. Torque-Torque Ripple Pareto Fronts

The potential of the new geometry was investigated via several MODE runs stopped at progressive numbers of iterations, to establish a relationship between the output performance and the computational time. A first set of 10 runs was stopped after 1200 function calls (1200 candidate machines evaluated). Other 10 runs were stopped at 3000 calls and, finally, a last set of 10 runs was stopped at 10000 evaluations. In Fig. 4 the three groups of ten Pareto fronts are summarized and directly compared with the ones obtained with the same MODE procedure and the simpler I2U geometry of Fig. 1a. Such geometry is representative of the two degrees of freedom per flux barrier case, as said in section II.

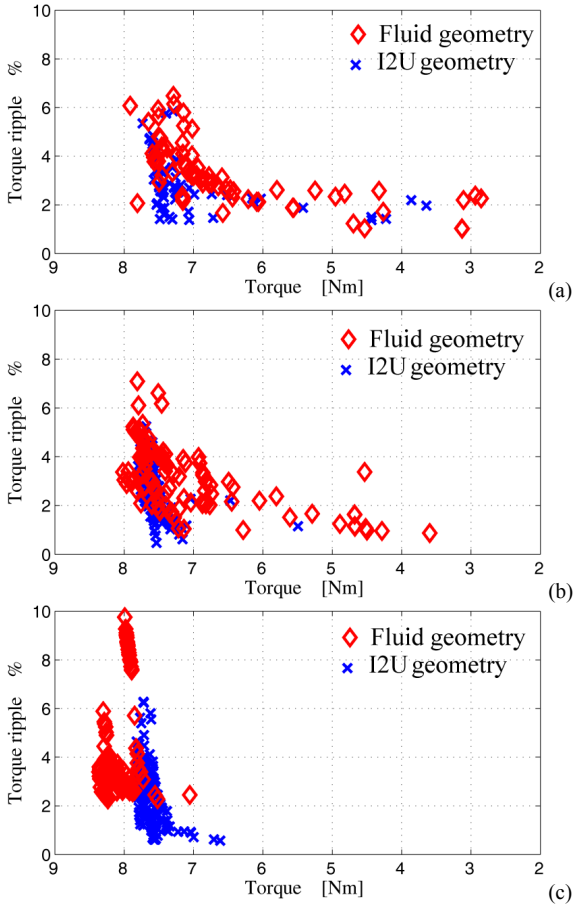

Figure 4. Summary of the Pareto fronts of 10 MODE runs for the fluid geometry (red) and the I2U geometry (blue). a) Stop after 1200 calls; b) 3000calls; c) 10000 calls.

The Pareto fronts in Fig 4a and Fig. 4b put in evidence that after 1200 calls and also after 3000 calls the

performance of the two geometries is still comparable. The aggregate of ten fronts of one geometry is fairly superimposed to the 10 fronts of the other geometry. In both subfigures, there are two mild but consistent trends: 1) the I2U rotors tend to have solutions with very lower ripple values, 2) the fluid barrier rotors tend to have solutions with higher torque values.

At 10000 calls, in Fig. 4c, the new fluid geometry has a clear advantage in terms of average torque, and the performance of the I2U solutions did not improve respect to the situation at 3000 calls. In other words, the further calls from 3000 to 10000 (Fig. 4b to 4c, blue markers) are unnecessary for the I2U rotors. In turn:

- The 2 x n_{lay} parameters geometry (I2U) converges to its maximum performance in a shorter time.
- Coherently, the 3 x n_{lay} parameters geometry (fluid barriers) can give a better performance, at the expense of a longer computational time.
- Comfortably enough, the performance obtainable with the new geometry and quick runs (1200 and 3000 calls) is not worse than the one obtained before.

A last remark is dedicated to the torque ripple. The I2U geometry has solutions with very low ripple values, unmatched by the fluid barrier geometry. This is neither a consequence of the number of degrees of freedom nor the different barriers profiles in the two cases. To the authors experience, after many extra-runs not reported in this paper, this is related to the shapes of the barriers ends, and the regular semicircular shapes of Fig. 1a showed to permit low ripple figures with a relative ease, whereas the more unpredictable shapes coming out from the fluid barrier approach (Fig. 1b) do not. The detailed investigation of this aspects is left out of this paper, in consideration of the good ripple values already obtainable with the fluid geometry in its present form, confirmed by the experiments. Otherwise said: the very low torque ripple range, between 1% and 2%, FEA predicted for the I2U rotors in Fig. 4 is not confirmed by the experiments, while the torque ripple figures around 2% expected from the fluid barriers in Fig. 4 are more consistent with the experimental results. Future work will be dedicated to the evaluation of the sensitivity of the cost functions (i.e. torque ripple) to the geometric parameters and to manufacturing uncertainties.

C. Non-Dominated Solutions

The non-dominated solutions taken from the sets of Pareto fronts of Figure 4 are considered in this section and summarized in Fig. 5. One solution to a multi-objective optimization problem is defined non-dominated when there is no other solution performing better in both (or all, for *n*-objectives) the cost functions. Each set of 10 MODE runs is considered time by time as a whole to produce a front of non-dominated solutions representative of those 10 runs. In Fig. 5a for example, the non-dominated solutions of the 10 runs stopped at 1200 calls are represented along with the non-dominated fronts stopped at 3000 and 10000 calls. This for the fluid barrier rotors. In Fig. 5b the same is done for the I2U rotor geometry.

The evolution of the non-dominated fronts in Fig. 5 confirms the conclusions of the previous subsection, in a form that is easier to visualize:

1) 3000 calls are enough for the I2U geometry but not for the fluid barriers;

2) with enough computational time, the fluid barriers can give more torque.

Returning to the analysis of the aggregated Pareto front estimates, they evidence a not-perfect repeatability of the final result. In particular for the earlier stops, the number of calls is insufficient for full convergence. Second, there is noise in the evaluation of the cost functions, so some solutions are found by coincidence and not repeated on the other fronts. Third, stochastic algorithms are always at risk of a false convergence, i.e. of converging to local minima, so one or more fronts out of ten can be non-optimal.

IV. Results of the Automated Design

A. Selection of the Optimal Solution

Two optimal designs, one per geometry, are extracted from the Pareto fronts to be prototyped and compared. The criterion for selecting one solution from the MODE results is to set a maximum a target ripple value of 2% and choose from the Pareto fronts accordingly, with some flexibility.

For example: for the fluid barrier case the 3000 calls front in Fig. 5a would produce a solution with 7.8 Nm and 2% ripple, whereas the 10000 calls front of non-dominated solutions would give no solution within the 2% ripple. Nevertheless, the machine of the front which is closer to 2% ripple has a torque of 8.2 Nm and it is then selected as final design of the fluid barrier case. So the final design is expected to give 8.2 Nm and 2.2% ripple at maximum current.

About the I2U rotor solutions, the selection of the exact 2% ripple machine would produce 7.7 Nm after 3000 calls and 7.8 Nm after the 10000 calls. However, the front of the 10000 call solutions in Fig. 5b includes many solutions with a lower ripple and nearly the same torque. So a very promising machine advocated of 7.8 Nm and 1.2% ripple by the FEA was selected for being prototyped.

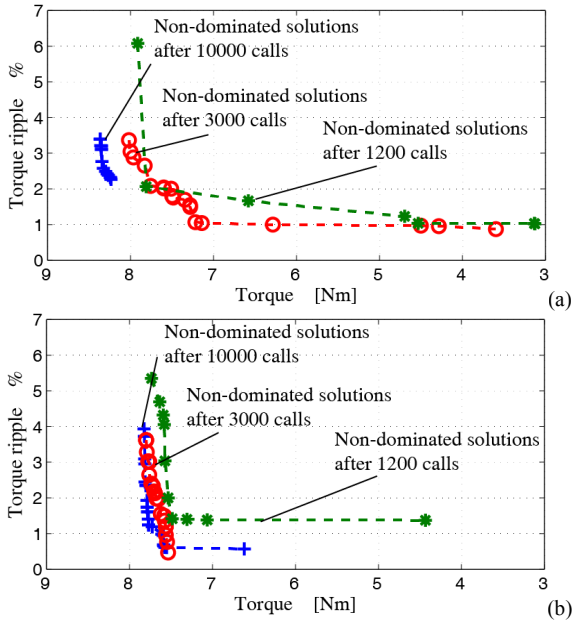

Figure 5. Envelope of non-dominated solutions of the 10 Pareto front groups of Fig. 4 for the two geometries: a) fluid barriers, b) I2U.

B. Discussion of the Two Optimal Solutions

The cross sections of the final designs, selected from the MODE results in Fig. 5, are represented in Fig 6. The blue circles indicate the positions of the barrier ends at the airgap. It is evident in both cases that the MODE found that the torque ripple is minimized by means of equally spaced

equivalent rotor "slots", as also found in the literature [5,17].

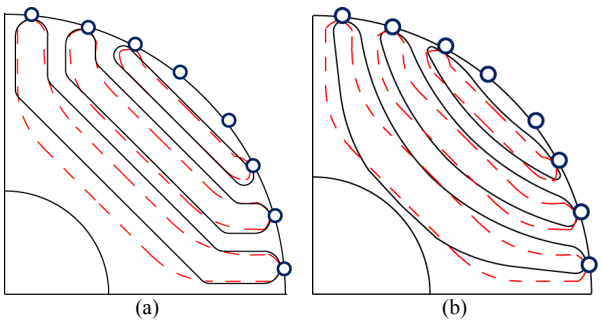

(a) (b)

Figure 6. Final MODE designs (black continuous lines) superimposed to the state of the art (SOA) rotor pole (red dashed lines). a) I2U, b) fluid.

The red dashed traces superimposed to the MODE designed cross sections are representative of the State of the Art (SOA) rotor prototype used for comparison in the following, designed according to the principles of [5]. Besides the same rotor slot positions, common to all three rotors, the fluid geometry (Fig. 6b) shows a good agreement with the SOA also in terms of the distribution of the flux barrier and flux channel thicknesses along the q-axis.

C. Flux Density Distribution

The flux density maps, FEA evaluated at rated current conditions, are reported in Fig. 7 for the three machines under comparison: the fluid and the I2U automatic designs and the SOA design. It is evident that the same current loading produces different grades of saturation in the rotor, for the three. The machines with more degrees of freedom (Figs. 7b and 7c) see their flux guides being less loaded. This thanks to the possibility of optimizing the thickness of the flux guides separately from the thickness of the flux barriers. The I2U geometry has no possibility in this sense, and its flux guides are more loaded already at continuous current (while the optimization was run at overload current). The earlier saturation justifies the lower output torque obtained with the I2U rotor, a problem that is overcome with the new fluid barriers.

V. Experimental Results

Three rotor prototypes were realized, wire-cut, and accommodated on two identical shafts to be replaced into a common stator. The pictures of the laminations are reported in Fig. 8.

A. Experimental Setup

A dedicated test bench was used to measure the torque waveforms of the prototypes in many different i_d, i_q current combinations. A speed-controlled DC motor having very low torque ripple drives the motor under test via a reduction gearbox. The speed is set to 10 rpm. The torque is measured via a high precision torque meter. The motor under test is vector-controlled, using a dSPACE 1104 R&D controller board. The i_d, i_q reference sequence and the acquisition of the torque signal during one motor revolution are automatically handled by means of a Matlab script using the commands of the MLIB/MTRACE dSPACE library [18] for dSPACE experiments automation. The torque-meter rating imposes to stay under 10 Nm which corresponds to an area of operation of 20 A per 30 A in the i_d, i_q plane. The test setup is depicted in Fig. 9.

B. Torque Comparison

At first, the average torque performance is considered. The measured torque values are represented for the three prototypes as a function of the current phase angle in Fig. 10. Three current amplitudes are represented, corresponding to 44%, 117% and 227% of the continuous current amplitude. Phase angle zero means that the current vector is aligned to the d-axis, whereas phase angle 90° corresponds to the q-axis. The 32.5 A condition is also the one used by the MODE for producing the automated designs. In Fig. 10, the three torque curves at low current are identical. As the current grows, the "fluid" machine has a progressive advantage over the SOA prototype, which has an advantage over the I2U prototype.

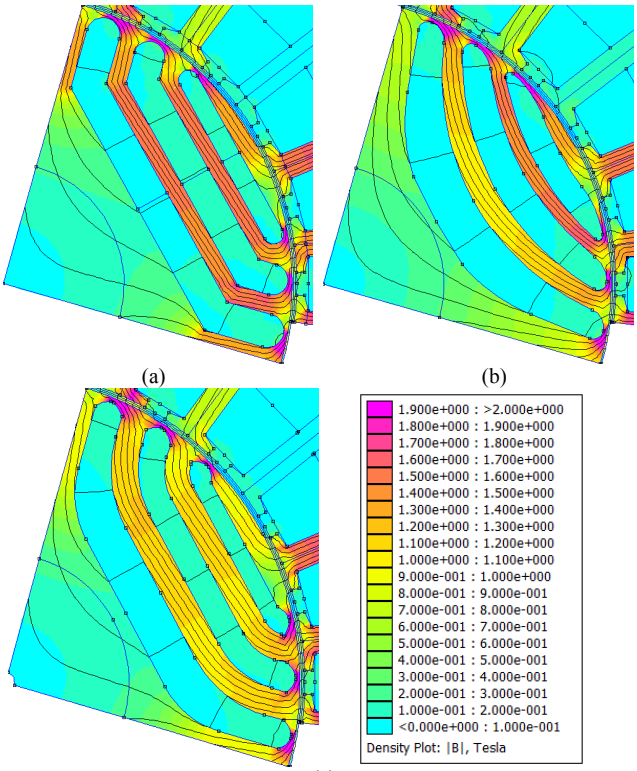

(a) (b) (c)

Figure 7. Flux density maps for the three motors under analysis, at continuous current and MTPA conditions. a) I2U; (b) Fluid barrier; (c) SOA.

(a) (b) (c)

Figure 8. Rotor laminations. a) Fluid barriers; b) I2U; c) SOA.

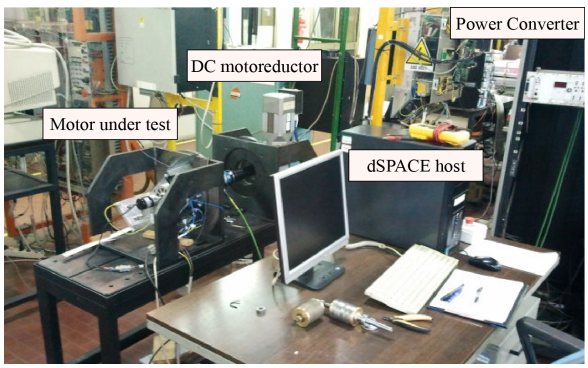

Figure 9. Test bench used for the identification of the prototypes.

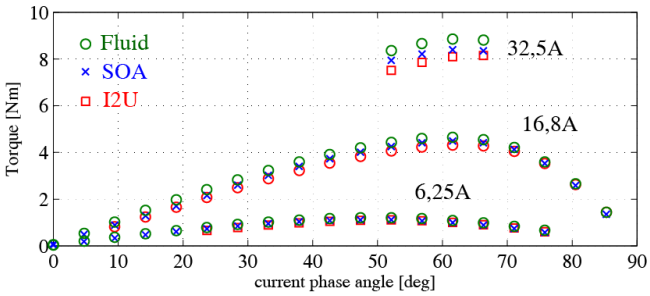

Figure 10.Comparison of the measured average torque as a function of the current phase angle at current amplitudes 6.5 A (44%), 16.8 A (117%) and 32.5 A (227%).

This confirms that the latter machine is the one suffering more from progressive steel saturation. The torque improvement from the 2 x n_{lay} parameters geometry (I2U) to the 3 x n_{lay} parameters fluid geometry is confirmed by the experiments. Plus, the new geometry can have more torque that a standard design.

It is important to remark that the SOA machine was not specifically optimized for maximum torque, and also that a human design cannot explore all the space of the design parameters to find the exact maximums of all the design goals. So to say that the better torque obtained with the fluid barrier geometry here indicates that ***the torque obtainable with three parameters per flux barrier is comparable to the one obtainable with no restrictions to the rotor barriers description***. The MODE-designed machine then has a higher torque thanks to the application of the optimization algorithm.

In conclusion, the proposed approach defines a description of the SyR rotor geometry that is arguably the simplest form of obtaining the maximum possible torque performance.

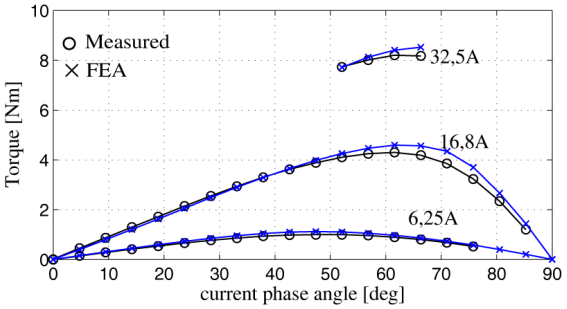

Figure 11. I2U rotor prototype: FEA versus measured torque.

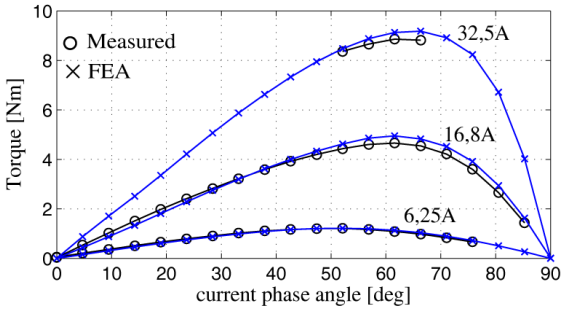

Figure 12. Fluid rotor prototype: FEA versus measured torque.

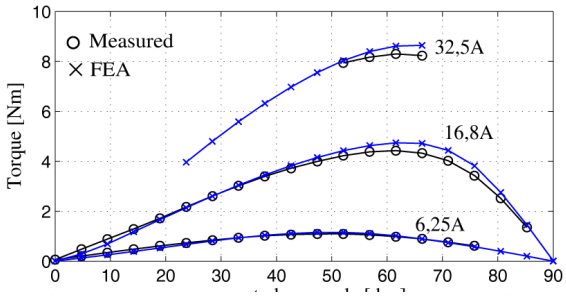

Figure 13. SOA rotor prototype: FEA versus measured torque.

C. *Measured Versus FEA Calculated Torque*

The measured torque values are compared to the FEA calculated ones in the graphs in Figs. 11 to 13. For all the machines the discrepancy between calculations and experiments is little and always in favor of the FEA results. This is somehow expected and can have different justifications: the non-exact knowledge of the steel properties, the effect of cutting over the ideal B-H curve of the steel, the manufacturing tolerances, the 3-dimensional effects not accounted for in the 2-dimensional simulation.

D. *Torque Ripple Comparison*

The measured and FEA calculated torque waveforms are reported in Figs. 14 to 16 for the three machines. One electrical period (half mechanical revolution) is represented. The same three current levels used in the previous figures are used here, in the respective MTPA conditions. The FEA and measured values are directly compared. The experiments confirm that the torque ripple of the fluid barrier-, automatic design is fairly minimized and lower than the one of the SOA design (Figs. 15 and 16, respectively). This again is due to the application of the optimization algorithm.

The FEA and experimental curves are generally close to each other, with the exception of the I2U prototype (Fig. 14), where the discrepancy grows with the load. Tests on a second prototype are scheduled, for possibly eliminating such discrepancy. It is still true that the lower ripple potential of the I2U forecasted by the FEA (Fig. 4c and Fig. 5) is not verified in practice. The additional results on the second I2U prototype will be integrated into the final paper.

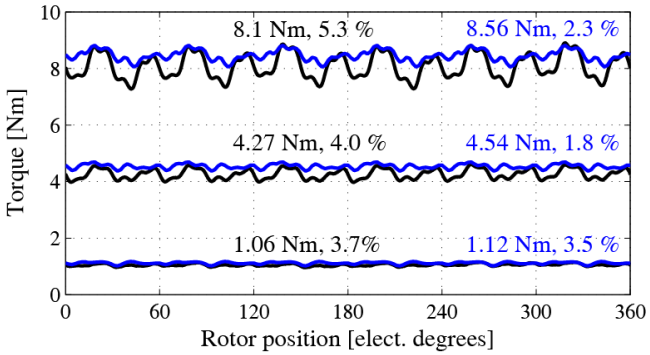

Figure 14. Prototype I2U: torque waveforms at the same current amplitudes of Fig. 10, in MTPA conditions. Blue: FEA; Black: Experimental.

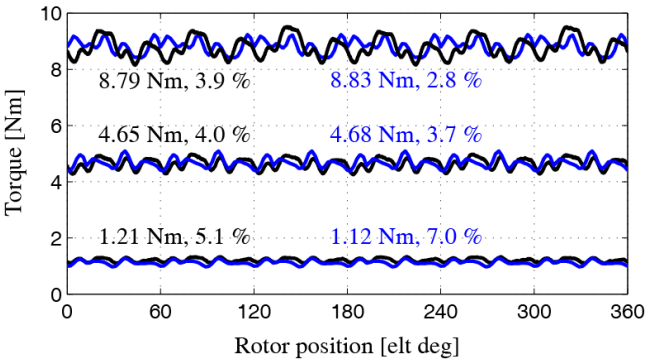

Figure 15. Prototype Fluid: torque waveforms at the same current amplitudes of Fig. 10, in MTPA conditions. Blue: FEA; Black: Experimental.

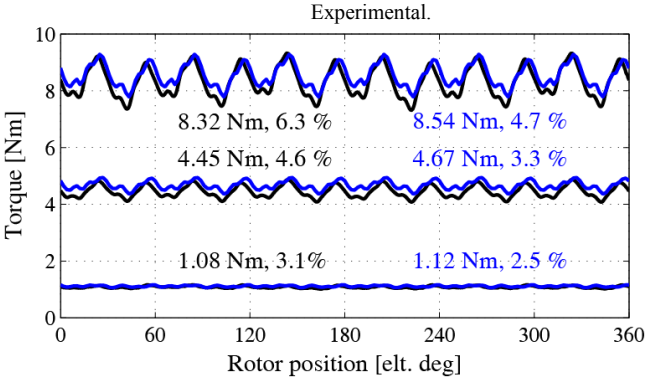

Figure 16. Prototype SOA: torque waveforms at the same current amplitudes of Fig. 10, in MTPA conditions. Blue: FEA; Black: Experimental.

In turn, the automatically designed rotor proposed in this paper can improve the torque and torque ripple performance of previous automated designs and also the typical values of state of the art designs.

VI. Conclusion

This work demonstrates that an automatic designed SyR rotor described with three geometric parameters per flux barrier can perform better than a human-designed prototype, which has no limits to the degrees of freedom for the description of its rotor geometry. The proposed fluid-barrier geometry improves the results obtained in the previous works dedicated to the automatic design of SyR machines and will be the pivot of a fully automated, time competitive design procedure for this class of synchronous machines, to the benefit of the industrial world.

References

[1]. T. A. Lipo, T. J. E. Miller, A. Vagati, I. Boldea, L. Malesani, and T. Fukao, “Synchronous reluctance drives,” in Conf. Rec. IEEE IAS Annu. Meeting, Denver, CO, Oct. 1994.

[2]. Moghaddam, R.R.; Magnussen, F.; Sadarangani, C.; , "Theoretical and Experimental Reevaluation of Synchronous Reluctance Machine," Industrial Electronics, IEEE Transactions on , vol.57, no.1, pp.6-13, Jan. 2010

[3]. Ooi, S.; Morimoto, S.; Sanada, M.; Inoue, Y., "Performance Evaluation of a High-Power-Density PMASynRM With Ferrite Magnets," Industry Applications, IEEE Transactions on , vol.49, no.3, pp.1308,1315, May-June 2013.

[4]. Staton, D.A.; Miller, T.J.E.; Wood, S.E., “Maximising the saliency ratio of the synchronous reluctance motor,” Electric Power Applications, IEE Proceedings B , vol.140, no.4, pp.249,259, Jul 1993.

[5]. A. Vagati, M. Pastorelli, G. Francheschini, and S. Petrache, “Design of low-torque-ripple synchronous reluctance motors,” Industry Applications, IEEE Transactions on, vol. 34, no. 4, pp. 758 -765, Jul/Aug 1998.

[6]. Kamper, M.J.; van der Merwe, F.S.; Williamson, S., ”Direct finite element design optimisation of the cageless reluctance synchronous machine”, IEEE Transactions on Energy Conversion, Vol. 11, n. 3, September 1996.

[7]. Sung Ju Mun; Yong Hyun Cho; Jung-Ho Lee, “Optimum Design of Synchronous Reluctance Motors Based on Torque/Volume Using Finite-Element Method and Sequential Unconstrained Minimization Technique,” Magnetics, IEEE Transactions on , vol.44, no.11, pp.4143,4146, Nov. 2008.

[8]. Yao Duan; Ionel, D.M., "A Review of Recent Developments in Electrical Machine Design Optimization Methods With a Permanent-Magnet Synchronous Motor Benchmark Study," Industry Applications, IEEE Transactions on , vol.49, no.3, pp.1268,1275, May-June 2013

[9]. Vagati, A.; Canova, A.; Chiampi, M.; Pastorelli, M.; Repetto, M., “Design refinement of synchronous reluctance motors through finite-element analysis,” Industry Applications, IEEE Transactions on , vol.36, no.4, pp.1094,1102, Jul/Aug 2000

[10]. Pellegrino, G.; Cupertino, F., "FEA-based multi-objective optimization of IPM motor design including rotor losses," IEEE Energy Conversion Congress and Exposition (ECCE), 2010, vol., no., pp.3659-3666, 12-16 Sept. 2010

[11]. Cupertino, F.; Pellegrino, G.; Gerada, C., “Design of synchronous reluctance machines with multi-objective optimization algorithms,” Energy Conversion Congress and Exposition (ECCE), 2013 IEEE , vol., no., pp.1858,1865, 15-19 Sept. 2013.

[12]. Pellegrino, G.; Cupertino, F.; Gerada, C., “Barriers shapes and minimum set of rotor parameters in the automated design of Synchronous Reluctance machines,” Electric Machines & Drives Conference (IEMDC), 2013 IEEE International , vol., no., pp.1204,1210, 12-15 May 2013.

[13]. Zarko, D.; Ban, D.; Lipo, T.A., "Design optimization of interior permanent magnet (IPM) motors with maximized torque output in the entire speed range," Power Electronics and Applications, 2005 European Conference on.

[14]. Sizov, G.Y.; Ionel, D.M.; Demerdash, N.A.O.; , "Multi-objective optimization of PM AC machines using computationally efficient - FEA and differential evolution," Electric Machines & Drives Conference (IEMDC), 2011 IEEE International , vol., no., pp.1528-1533, 15-18 May 2011

[15]. David Meeker, “Finite Element Method Magnetics”, Ver. 4.2 User’s Manual, February 5, 2009, [Online] available: http://www.femm.info/Archives/doc/manual.pdf.

[16]. K.J. Binns, P.J. Lawrenson, C.W. Trowbridge, ”The analytical and numerical solution of electric and magnetic fields”, John Wiley and Sons copyright 1992.

[17]. RR Moghaddam, “Rotor for a Synchronous Reluctance Machine”, US Patent App. 13/230,543, 2011

[18]. http://www.dspace.com.

Biographies

Matteo Gamba received the M.Sc. in electrical engineering from the Politecnico di Torino, Turin, Italy in 2011. He is currently working toward his PhD in electrical engineering with the same university. His PhD research project deals with the design of Synchronous Reluctance and PM-assisted Synchronous Reluctance machine drives.

Gianmario Pellegrino, received the M.Sc. and Ph.D. degrees in electrical engineering from the Politecnico di Torino, Turin, Italy, in 1998 and 2002, respectively. Since 2002 he is with Politecnico di Torino. His research interests include the design of electrical machines and the control of electrical drives. He is involved in research projects with industry and has more than 20 journal papers and one patent. Dr. Pellegrino is an Associate Editor for the IEEE Transactions on Industry Applications and an IEEE Senior Member. He is the co-recipient of three Prize Paper Awards. He was a guest researcher at Aalborg University, Denmark, in 2002, a visiting fellow at Nottingham University, UK, in 2010/2011, and an honorary fellow at the University of Wisconsin-Madison, USA, in 2013.

Francesco Cupertino, received the Laurea degree and the PhD degree in Electrical Engineering from the Politecnico di Bari, Italy, in 1997 and 2001 respectively. From 1999 to 2000 he was with PEMC research group, University of Nottingham, UK. Since July 2002 he is an Assistant Professor at the Politecnico di Bari, Electrical and Electronic Engineering Department. His research interests include the design of permanent magnet electrical machines, intelligent motion control, and applications of computational intelligence to control and design. He is the author or co-author of more than 90 scientific papers. He is the scientific director of the laboratory Energy Factory Bari (EFB), a joint initiative of the Politecnico di Bari and AVIO AERO GE, aimed at developing research projects in the fields of aerospace and energy. He is an IEEE senior member.